WILEY

Electron cloud spin generated by microring space-time control circuit for 3D quantum printing

Arumona Edward Arumona[1,2,3] |
Suphanchai Punthawanunt[4] | **Kanad Ray**[5] |
Sirigiet Phunklang[6] | **Preecha Yupapin**[1,2] 🆔

[1]Computational Optics Research Group, Advanced Institute of Materials Science, Ton Duc Thang University, District 7, Ho Chi Minh City, Vietnam

[2]Faculty of Applied Sciences, Ton Duc Thang University, District 7, Ho Chi Minh City, Vietnam

[3]Division of Computational Physics, Institute for Computational Science, Ton Duc Thang University, District 7, Ho Chi Minh City, 700000, Vietnam

[4]Faculty of Science and Technology, Kasem Bundit University, Bangkok, 10250, Thailand

[5]Amity School of Applied Sciences, Amity University, Jaipur, Rajasthan, India

[6]School of Telecommunication Engineering, Institute of Engineering, Suranaree University of Technology, Nakhon Ratchasima, Thailand

Correspondence
Preecha Yupapin, Computational Optics Research Group, Advanced Institute of Materials Science, Ton Duc Thang University
District 7, Ho Chi Minh City, Vietnam.
Email: preecha.yupapin@tdtu.edu.vn

Abstract

A three-dimensional (3D) quantum printing technique is proposed that uses electron spin cloud projections generated by microring-embedded gold grating. A dark soliton pulse with a center wavelength of 1.50 μm excites the gold grating, leading to electron cloud oscillations. By using suitable parameters, the whispering gallery mode is obtained, which is the result of trapping light (electrons) inside the silicon microring. The plasma wave frequency is generated at the Bragg wavelength at which the electron density is obtained. The electron spin-down and spin-up forms the x-axis and y-axis along the propagation z-axis. In this proposal, the propagation wave axis is applied to increase the printing resolution. The printing points are formed by the spin-down, spin-up, and no spin associated with [x, y, z] as [1, 0, −]. The electron spins are distinguished by the time sequence and by modulating with the Gaussian pulse of 1.30, 1.10, and 0.80 μm,

from which the spin states of the electron can be detected and characterized. The shortest space-time paradox gap is around 50 fs, which is the limitation of all measurements (observations). The electron transport spin projection is achieved with respect to the time function in which the 3D image is printed with a resolution of 50 fs (10^{-15} s). In application, the trapped electron densities within the circuit are made possible via wireless connection for long-distance transmission.

1 | INTRODUCTION

Three-dimensional printing (3D) is also called additive manufacturing and involves creating 3D solid objects from a digital file. This starts with the fabrication of 3D objects layer by layer directly from computer-aided design (CAD) drawings. It can be used to create complex shapes or designs of objects by using 3D modeling software. The objects' fabricated layers are printed using a 3D printer,[1] and the first thing needed for 3D printing is 3D modeling software. The working principle of a 3D printer is similar to that of an inkjet printer, where the 3D models are built layer upon layer from the bottom upward by printing over the same area repeatedly. The printer builds the 3D model directly from the 3D CAD drawing using many two-dimensional (2D) prints that sit on top of one another without paper in between. The printer does not apply ink to the deposit of the molten plastic layer, whereas the 2D prints that sit on top of one another are joined together to create the 3D object. There are different methods used for 3D printing, including vat photopolymerization, material jetting, binder jetting, material extrusion, powder bed fusion, sheet lamination, and directed energy deposition. A 3D printer that uses vat photopolymerization and material jetting methods makes use of ultraviolet light in the hardening or fabrication of 3D structural objects.[2] Other techniques have been employed by different researchers in printing 3D color objects.[3-8] For example, Yejing et al[9] used photonic crystals and heat-shrinking techniques in the printing of 3D structural color objects at a microscopic scale. Jingfang et al[10] developed a bis furan cyclohexane derivative/polyethylene glycol

diacrylate photoinitiator system. It has excellent photobleaching performance, which is being employed for 3D light color printing for a long-wavelength light-emitting diode. However, searching for a new technique that can provide a better printing resolution has continued. In the current study, a novel 3D color printing technique that makes use of electron cloud spin projections has been proposed and manipulated. The microring circuit has the form of a panda ring, which has been used by many researchers for different applications. The advantage is that the nonlinear phase modulators can be adjusted to obtain the whispering gallery mode (WGM), which is suitable for the required applications.[11-14] The WGM phenomenon has been used by different researchers for various applications.[15,16] The electron cloud is the region where electrons are most likely to be localized. Many researchers have used the concept of controlling the electron spin for various applications.[17] In this proposed technique, the nonlocalized electron propagation along the z-axis is also included to increase the printing resolution, and promising results have been obtained. The Optiwave program has been used for the simulation from which the parameters are extracted, and the MATLAB program makes use of the extracted parameters. The MATLAB program implements 3D quantum printing that uses electron cloud spin projections generated by the microring circuit.

2 | BACKGROUND

The electron has a quantum feature known as spin. The electron spins in 3D are considered.[18] In the x-axis: spin-down $|\downarrow> (|1>)$, with the spin matrix is $\frac{\hbar}{2}\begin{vmatrix} 0 & 1 \\ 1 & 0 \end{vmatrix}$. In y-axis: spin up $|\uparrow> (|0>)$, with the spin matrix is $\frac{\hbar}{2}\begin{vmatrix} 0 & -i \\ i & 0 \end{vmatrix}$, and for the z-axis: the propagation axis, which is the probability of spin up or spin down, which is given by is $C_1|\uparrow> + C_2|\downarrow>$. The probability of spin up is $|C_1|^2$, whilethe probability of spin down is $|C_2|^2$, Thus, the probability of spin up or spin down is $|C_1|^2 + |C_2|^2 = 1$, with the spin matrix $\frac{\hbar}{2}\begin{vmatrix} 1 & 0 \\ 0 & -1 \end{vmatrix}$, where C_1 and C_2 are constants. $\hbar$ is the reduced Planck's constant. The superposition can be any of the two states, which is written as $|\psi> = \alpha|0> + \beta|1>$, with $|\alpha|^2 + |\beta|^2 = 1$.

The schematic diagram of the microring circuit is shown in Figure 1A, where the space source input is the dark soliton pulse,[22] with the wavelength $\lambda_1$as given in Equation (1) in terms of $\omega = 2\pi\frac{v}{\lambda}$. Similarly, the modulated source is the Gaussian pulse with wavelength λ_2 as given in Equation (2). The fabrication structure is shown in Figure 1B, which consists of the silicon substrate, two silicon linear waveguides, a silicon microring at the center, with two nanorings at its sides. The center of the silicon microring is embedded with gold grating, which gives rise to electrons when illuminated
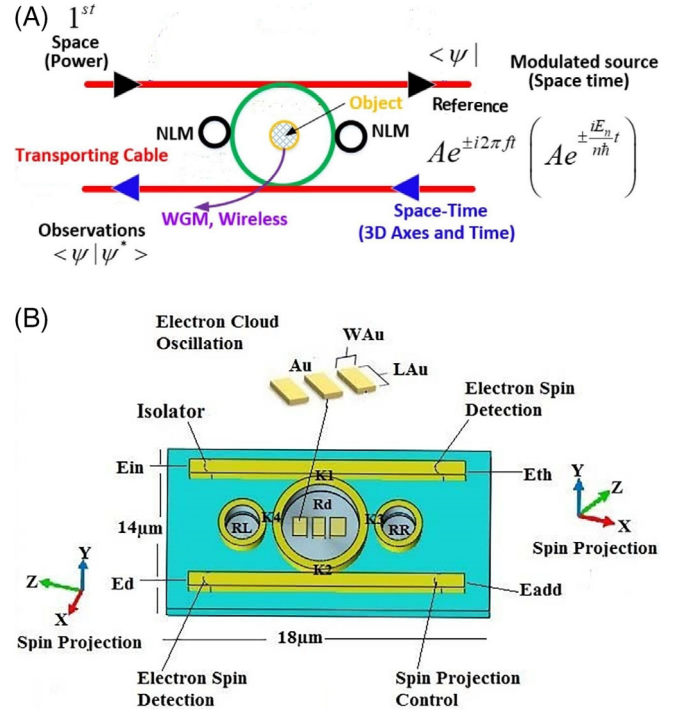

FIGURE 1 A, Schematic diagram of the 3D quantum printing circuit, where NLM is the nonlinear phase modulator, WGM is the whispering gallery mode. The first space power can be the soliton pulse at the input port, the modulated source can be the Gaussian pulse at the add port. B, The fabrication structure, where the input port, throughput port, add port, and drop port are E_{in}, E_{th}, E_{add}, and E_d, respectively. R_d: main ring radius, R_R and R_L: side ring radii, K1-K4: coupling constants. The isolator and spin projection control are applied to protect the feedback and filtering purpose. The other symbols are given in Table 1 [Color figure can be viewed at wileyonlinelibrary.com]

by light and the behavior of the electrons described by the Drude model[22,23] as written in an Equation (3).

$$\Psi = Be^{-i\left(\omega t + \frac{E_n}{n\hbar}t\right)},\quad(1)$$

where $B = \bar{B}.\text{Tan}h\left(\frac{T}{T_0}\right)\exp\left(\frac{z}{2L_D}\right)$, which is the input field (dark soliton). $\bar{B}$ is the amplitude, z is the propagation distance, T is the propagation time of the soliton pulse, the length dispersion $L_D = \frac{T_0^2}{\beta}$, where T_0 is the initial propagation time, β is the propagation constant in linear and nonlinear terms.[24] ωt is the phase term of the multiplexing function, $\frac{E_n}{n\hbar}$, $n = 1, 2, 3,...$

The multiplexed space-time applied into the system, which is given by an Equation (2).

$$E_{add} = Ae^{\pm i\omega t}\quad(2)$$

where $\omega = 2\pi f, f = \frac{c}{\lambda_2}, \omega, f, \text{and} c$ are the angular frequency, linear frequency and speed of light in vacuum, respectively. D and t are the amplitude and time, respectively. The $\pm$ signs of the exponent term used for the full-time slot axis; the control time is given by $e^{\pm i\omega t}$ and $t = 0$ for the time domain.

$$\epsilon(\omega) = 1 - \frac{ne^2}{\epsilon_0 m \omega^2} \qquad (3)$$

The relative permittivity defined by ϵ_o, electron charge defined by e, mass defined by m and electron density defined by n and angular frequency defined by ω_p. At resonance, the angular frequency becomes plasma frequency (ω_p) as written in Equation (4) as:

$$\omega_p = \left[\frac{ne^2}{\epsilon_0 m}\right]^{-\frac{1}{2}} \qquad (4)$$

From Equation (4) the electron density $n = \frac{\omega_p^2}{e^2}\epsilon_0 m$. The plasmonic wave oscillation is a consequence of electron density in an electric field. To obtain the exponent decay and TM-polarization of the electric field Maxwell equations are employed.

The Bragg and resonant wavelengths are related by $\lambda_B = 2n_e\Lambda$, Bragg wavelength is λ_B, effective refractive index is n_e, which is also the refractive index of the gold gratings inside the waveguide and grating period is Λ. Kerr effect exists through the structure and it can be included in the $n = n_0 + n_2$, $I = n_0 + n_2$, P/A_{eff} equation. n is the refractive index, n_0 is the linear refractive index, n_2 is the nonlinear refractive index, I is the optical intensity, P is the optical power and A_{eff} is the structure effective mode core area. The two nanorings at the sides of the silicon microring act as phase modulators which control the whispering gallery mode at resonance and through the throughput and drop ports the normalized intensities are obtained. The normalized intensities of the system output written as[14]:

$$\frac{I_{th}}{I_{in}} = \left[\frac{E_{th}}{E_{in}}\right]^2 \qquad (5)$$

$$\frac{I_{drop}}{I_{in}} = \left[\frac{E_{drop}}{E_{in}}\right]^2 \qquad (6)$$

From Equations (5) and (6), the first apace function is a soliton input via an input port, while the second space-time function is input via the add port simultaneously. The successive filtering of the transmission circuit controlled by the two side ring coupling parameters, where the induced nonlinear effects coupled the center ring can give the resonance. Finally, the spin projection applied at the resonance condition at the drop port, while the throughput formed the reference port. The spins transport can apply using the WGM and throughput port output for long-distance transmission, in which the spin information transmits via the spin-waves into the transmission lines.

3 | RESULTS AND DISCUSSION

In the simulation, the schematic and fabrication structure is as shown in Figure 1.[25] The input light (dark soliton) fed into the system has a center wavelength of 1.50 μm via the
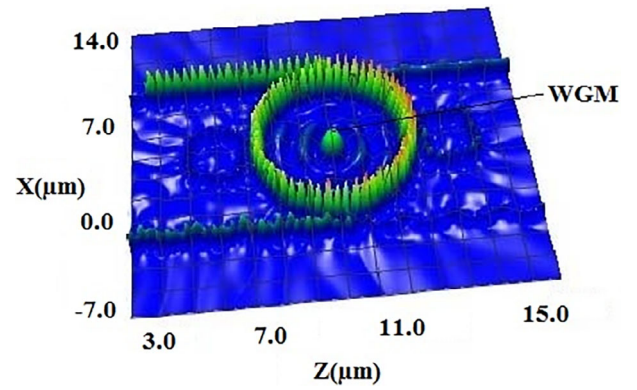

FIGURE 2 Results of the graphical output of the Opti-wave program, with the formation of the whispering gallery mode (WGM) at the center of the main ring of the microring circuit, where $R_d = 3.0$ μm, $R_R = 1.0$ μm, $R_L = 1.0$ μm, each κ = 0.50, Input power = 25 mW, with the center wavelength of 1.50 μm, and other parameters given in Table 1 [Color figure can be viewed at wileyonlinelibrary.com]

input port. The gold grating at the center ring is excited by the input light, where the Bragg wavelength formed. The oscillation of the polariton dipoles and plasmonic waves occurs. The generated whispering gallery mode is made possible from the coupling of light inside the microring with the embedded gold gratings at the center of the silicon microring. The center wavelength usually shifted by the gold grating to the Bragg wavelength. The device output ports are the throughput and drop ports, where the output signals are obtained. First, in the manipulation, the 32-bit version 12.0[26] of the Optiwave FDTD program is employed and at resonance with a particular wavelength results in the trapping of light inside the silicon microring. The grid size of the system using the Optiwave FDTD simulation is 0.05 with the mesh cell size of 399, 71, and 456 for the three axes (x, y, and z, respectively). The APML boundary condition which is the anisotropic perfect matched layer is used with a layer of 15, real tensor of 1.0 and 1.0×10^{-12} theoretical reflection coefficient. The number of round trips is 20 000 which is used to confirmed resonant results. A high-performance computer of 32Gb RAM used for all simulations to ensure accuracy. As shown in Figure 2 is the WGM formed at the center of the silicon microring using other parameters in Table 1. The parameters from the results of the Optiwave FDTD simulation are extracted and used in the MATLAB program. In Figure 3, the plot of the electron spins with the time function is shown, where the spin-up (blue) at the throughput port, spin-down (red) at the drop port, and no spin (green) at the throughput port/drop port. Figure 3A is the modulation wavelength of 1.40 μm with a projection time of 1.50 fs. Figure 3B is the modulation wavelength of 1.10 μm with a projection time of 1.40 fs, while Figure 3C is the modulation wavelength of 0.8 μm with a projection time of 0.8 fs. The spins of the electron in three axes (x, y, z) given by the following. The spin to the x-axis (spin-x), y-axis, and z-axis are the spin-down|1>, spin-up|0>, and no spin projection,

TABLE 1 The parameters that were selected and used in the simulation

Parameters	Symbols	Values	Units
Input power (Dark soliton)	P	1–25	mW
Input power (Gaussian pulse)	P	1–25	mW
Length of silicon linear waveguide	L	15.0	μm
Silicon center ring radius	R_d	3.0	μm
Left nanoring radius	R_L	1.0	μm
Right nanoring radius	R_R	1.0	μm
Gold dielectric constant[19]	ϵ_o	6.9	
Gold permittivity[19]	ϵ	10.0	
Gold width	W_{AU}	0.4	μm
Gold thickness	d	0.2	μm
Gold length	L_{AU}	1.6	μm
Refractive index of Au[19]	n	1.80	
Insertion loss	γ	0.01	
Coupling coefficient	κ	0.50	
Refractive index Si[20]	n_{Si}	3.42	
Si nonlinear refractive index[20]	n_2	1.3×10^{-13}	$m^2 W^{-1}$
Input light wavelength input port	λ_1	1.50	μm
Modulation wavelength input	λ_2	1.40, 1.10, 0.80	μm
Waveguide core effective[20]	A_{eff}	0.30	$μm^2$
Waveguide loss	α	0.50	dB $(cm)^{-1}$
Plasma frequency[21]	ω_p	1.2990×10^{16}	rad s^{-1}
Electron mass	m	9.11×10^{-31}	kg
Electron charge	e	1.6×10^{-19}	Coulomb
Permittivity of free space	ϵ_o	8.85×10^{-12}	Fm^{-1}
Grating period	Λ	0.50, 0.40, 0.30	μm
Reduced Planck's constant	$\hbar$	1.00	ARU

respectively. By using Equations (1-6), the dark soliton pulse excites the gold grating, which leads to electron cloud oscillations. It can process the spin-up, and spin-down by the projection automatically at the drop port. The output at the throughput port performed the referencing information. The center wavelength of 1.50 μm when modulated with the Gaussian pulse of 1.30, 1.10, and 0.80 μm the spin states of the electron can be detected and characterized. The normalized outputs are obtained at the throughput and drop ports. The electron cloud at the center system is of high density due to the intense optical power at the center WGM. Figure 3D is the selected plot of the 3D image ($\lambda = 1.50$ μm) with the time function, where the 3D image resolution and filtering were taken in account. Generally, the projection of the first space to the second space after the singularity is linked by time-bridge. The paradox pair (orthogonal components) has the shortest time of the paradox gap. After the measurement (disturbance), the time-bridge broken, the paradox pair collapsed. The shortest time of the paradox pair is

around 50 fs. It is the limitation of all measurements (observations). The resolution obtained with an angle of observation of 45°, making use of the relation as $t = \left(\frac{\pi r n}{2c}\right)$, where t is the resolution at each projection point, r is the radius of the microring, n is the refractive index of the silicon ring, and c is the speed of light in vacuum. The separation of each spin projection point in time of 50 fs (10^{-15}s) achieved. For the 3D image construction, the grating at the center of the microring with suitable parameters in Table 1 forms the WGM beam, which is projected upwards and with the trapped electrons at the center, the electron cloud oscillation that leads to spin-down (red) and spin-up (blue) projected at the x and y axes propagated along the z-axis (green) are superimposed to construct the 3D image. The image formed by the vortex beam of the spin electrons, which is the twisted beam of the angular momentum. It appears as a helix surrounding a propagation beam (z-axis), which is projected on the flat surface, where the 3D image is constructed. For filtering, the median filter employed to remove the noise from the 3D image to
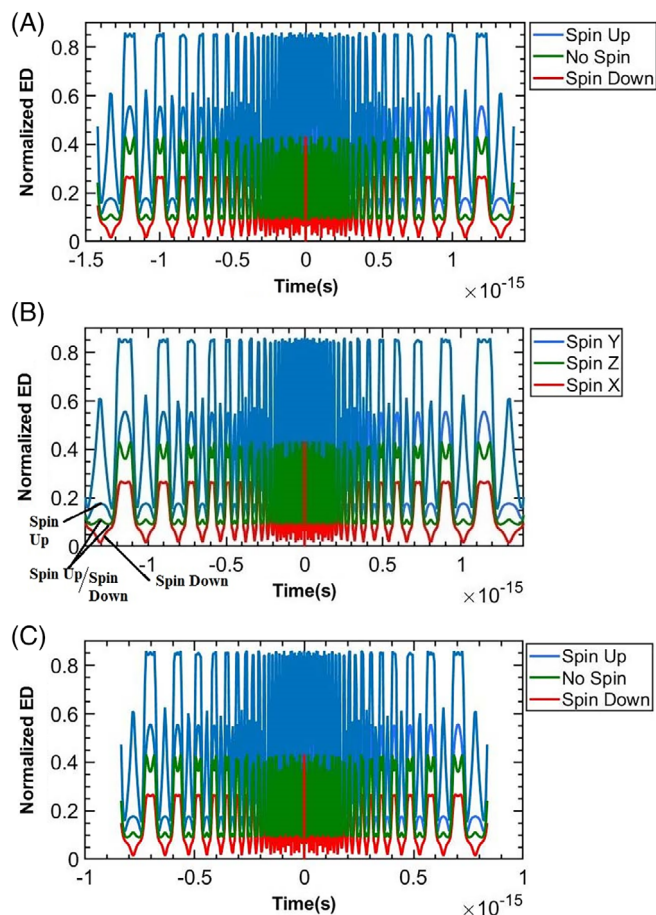
FIGURE 3 The plot of the Matlab program result using the time function where the spin-up (blue) at the throughput port, spin-down (red) at the drop port and spin-up/spin-down (green) at the throughput port/drop port, where A, the modulation wavelength of 1.40 μm with projection time of 1.50 fs; B, the modulation wavelength of 1.10 μm with projection time of 1.40 fs; and C, the modulation wavelength of 0.8 μm with projection time of 0.8 fs [Color figure can be viewed at wileyonlinelibrary.com]

enhance the 3D image quality. By using the MATLAB program, the filtering image by a 3 × 3 filter obtained. The trapped electron cloud distributed covering the gold grating at the center, which is in the form of WGM output. The electron transported sequentially in time to the projection target, which can be projected to the image plane, while the gap of the 2-spin projections filled by the non-spin along the propagation axis. In application, the electron cloud can be used to form a 3D shape (hollow), from which the 3D mold can be constructed and used for 3D printing. Moreover, this method is formed by the quantum network, which can also be applied by either wireless or cable transmission for long-distance transmission. By using the space-time control, where somehow the system can reach the teleportation when the space-time uncertainty saturation, which can also be very interesting and challenging for future technologies.

In operation, the microring embedded gold gratings circuit is used with an electron cloud spin projection to form the 3D image of the object at the center ring. A paradox pair

is formed by the wave-particle duality. After the projection, the measurement is observed. But the reality is disappeared, means the paradox pair is collapsed. The center ring radius is varied from 2 to 4 μm, where the results of 30, 50, and 70 fs scanning resolution are obtained by the ring radii of 2, 3, and 4 μm, respectively. The 3D image plot of these ring radii is shown in Figure 4A-C. The input light is the space source is fed into the system via the input port. The space-time source is multiplexed to form the space-time function at the add port. The input light (dark soliton) excites the gold gratings at the center ring, which leads to electron cloud oscillations that form the electron density results in the spin-up (y-axis) and spin-down (x-axis) of electrons, where both spins are propagating along the z-axis. The small rings at the side of the center ring act as phase modulators, induce the nonlinearity effect in the system. The trapped light oscillated around the microring inside the microring, the suitable parameters as given in Table 1. The trapped light forms the whispering gallery mode at the center ring, which is projected upwards and with the trapped electrons at the center ring where the spin-up (blue) (y-axis), and spin-down (red) (x-axis) propagating along the z-axis are superimposed to form the 3D image of the object at the center ring. Other works are cited in Table 2.

4 | CONCLUSION

A novel 3D quantum printing technique using a microring circuit has been proposed. The Bragg wavelength can be formed by the embedded gold grating which also induced polariton, which can be employed to form the plasmonic sensor and dipole oscillation. The electron cloud is driven by the polariton and generated in the form of the WGM beam, which can transport through the system via the space-time control carrier. The transport of the trapped electron densities within the circuit is made possible via wireless connection making use of the whispering gallery mode and via cable connection. The electron spins distinguished by the time sequence modulation and projection. By using the modulated sources with the Gaussian pulse of 1.30, 1.10, and 0.80 μm, the 3D images using the spin projections at the drop port obtained, in which the image projection space separation of 50 fs (10^{-15} s) is achieved. The 2-axes of the electron spins and the propagation axis use to form the image, where the 3D quantum printing can construct. In this study, the ground state of the electrons was only applied, which is described by the electron density. The errors were not taken in account since the errors have less effect on the quantum bits results. In application, a pan da-ring can form the plasmonic antenna and apply in a quantum computing device, quantum sensor, quantum encryption based on the spin projections, while the long-distance 3D image with quantum security via either cable or wireless is possible.
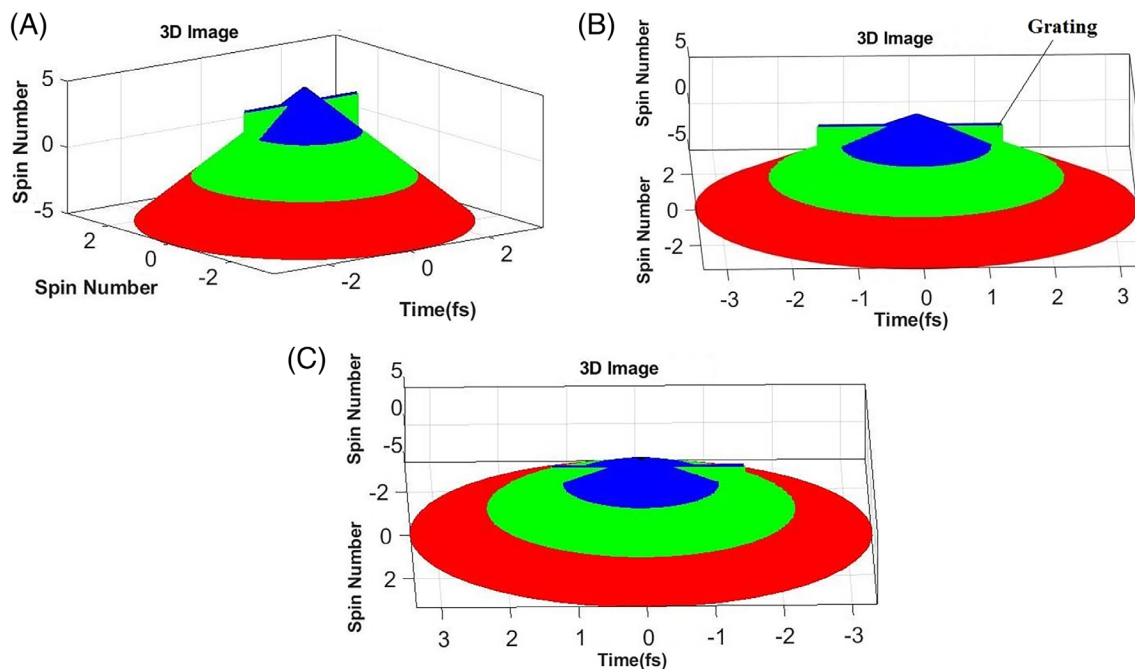
FIGURE 4   The 3D image plot ($\lambda = 1.50$ μm) using the electron transport spin projection with the modulation wavelength of 1.30 μm, where A, ring radius of 2 μm; B, ring radius of 3 μm; and C, ring radius of 4 μm [Color figure can be viewed at wileyonlinelibrary.com]

TABLE 2   Comparison of print resolution of present study with previous study

Proposed work (scanning resolution)	Other works
30 fs	1 ms^{-1} [27]
50 fs	40 mms^{-1} [28]
70 fs	8000 mms^{-1} [29]

CONFLICT OF INTEREST

The authors declare no conflict of interest.

ORCID

Preecha Yupapin https://orcid.org/0000-0002-6438-9276

REFERENCES

[1] Ni R, Qian B, Liu C, Liu X, Qiu J. 3D printing of resin composites doped with upconversion nanoparticles for anti-counterfeiting and temperature detection. *Opt Express*. 2018;26(19):1-11.

[2] Shahrubudin N, Lee TC, Ramlan R. An overview on 3D printing technology: technological, materials and applications. *Procedia Manuf*. 2019;35:1286-1296.

[3] Han T, Kundu S, Nag A, Xu Y. 3D printed sensors for biomedical applications: a review. *Sensors*. 2019;19(1706):1-22.

[4] Nesic A, Blaicher M, Hoose T, et al. Photonic-integrated circuits with non-planar topologies realized by 3D-printed waveguide overpasses. *Opt Express*. 2019;27(12):1-24.

[5] Ni R, Qian B, Liu C, Liu X, Qiu J. Three-dimensional printing of hybrid organic/inorganic composites with long persistence luminescence. *Opt Mater Express*. 2018;8(9):1-9.

[6] Huang Y, Zhu J, Fan J, et al. Plasmonic color generation and refractive index sensing with three-dimensional air-gap nano cavities. *Opt Express*. 2019;27(5):1-17.

[7] Guo H, Lv R, Bai S. Recent advances on 3D printing graphene-based composites. *Nano Mater Sci*. 2019;1:101-115.

[8] Hu Y, Luo X, Chen Y, et al. 3D-integrated metasurfaces for full-color holography. *Light Sci Appl*. 2019;8(86):1-9.

[9] Liu Y, Wang H, Ho J, et al. Structural color three-dimensional printing by shrinking photonic crystals. *Nat Commun*. 2019;10(4340):1-8.

[10] Li J, Hao Y, Zhong M, Tang L, Nie J, Zhu X. Synthesis of furan derivative as LED light photoinitiator: one-pot, low usage, photobleaching for light color 3D printing. *Dyes Pigm*. 2019;165:467-473.

[11] Koos C, Jacome L, Poulton C, Leuthold J, Freude W. Nonlinear silicon-on-insulator waveguides for all optical signal processing. *Opt Express*. 2007;15:5976-5990.

[12] A.H. Atabaki, S. Moazeni, F. Pavanella, H. Gevorgyan, J. Notaros, L. Alloatti, M.T. Wade, C. Sun, S.A. Kruger, H. Meng, K.A. Qubaisi, I. Wang, B. Zhang, A. Khilo, C. V. Baiocco, M.A. Popovic, V.M. Stojanovic, and R.J. Ram, "Integrating photonics with silicon nanoelectronics for next generation of system on a chip," *Nature* 556, 349–354(2018).

[13] Ali J, Pornsuwancharoen N, Youplao P, et al. Coherent light squeezing states within a modified microring system. *Results Phys*. 2018;9:211-214.

[14] Arumona AE, Amiri IS, Yupapin P. Plasmonic micro-antenna characteristics using gold grating embedded panda-ring circuit. *Plasmonics*. 2020;15:279-285.

[15] Punthawanunt S, Aziz MS, Phatharacorn P, Chiangga S, Ali J, Yupapin P. LiFi cross-connection node model using whispering gallery mode of light in a microring resonator. *Microsyst Technol*. 2018;24(12):4833-4838.

[16] Khomyuth C, Bahadoran M, Amiri IS, Youplao P, Pornsuwancharoen N, Yupapin P. Electric-optic conversion circuit incorporating a fiber optic loop for light fidelity up-down link use. *Microw Opt Technol Lett*. 2018;61(2):526-531.

[17] Bunruangses M, Youplao P, Amiri IS, et al. Electron cloud density generated by microring-embedded nano-grating system. *Plasmonics*. 2020;15:543-549.

[18] Russ M, Burkard G. Three-electron spin qubits. *J Phys Condens Matter*. 2017;29(393001):1-36.

[19] Pornsuwancharoen N, Amiri IS, Suhailin FH, et al. Micro-current source generated by a WGM of light within a stacked silicon-graphene-au waveguide. *IEEE Photon Technol Lett*. 2017;29(21):1768-1771.

[20] Prabhu AM, Tsay A, Han Z, Van V. Extreme miniaturization of silicon add-drop microring filters for VLSI photonics applications. *IEEE Photon J*. 2010;2(3):436-444.

[21] Blaber MG, Arnold MD, Ford MJ. Search for the ideal plasmonic nanoshell: the effects of surface scattering and alternatives to gold and silver. *J Phys Chem C*. 2009;113:3041-3045.

[22] Tunsiri S, Thammawongsa N, Threepak T, Mitatha S, Yupapin P. Microring switching control using plasmonic ring resonator circuits for super-channel use. *Plasmonics*. 2019;14:1669-1677.

[23] Prince G. Controlling level splitting by strong coupling of surface plasmon resonances with rhodamine-6G on a gold grating. *Plasmonics*. 2018;13(6):2067-2077.

[24] Agrawal GP. Nonlinear fiber optics: its history and recent progress [invited]. *J Opt Soc Am B*. 2011;28(12):A1-A10.

[25] Lu X, Li Q, Westly DA, et al. Chip-integrated visible-telecom entangled photon pair source for quantum communication. *Nat Phys*. 2019;15:373-381.

[26] OptiFDTD Technical Background and Tutorials (Finite Difference Time Domain) Photonics Simulation Software, Version 12.0. http://www.optiwave.com. Accessed September 20, 2019.

[27] Subramanian V, Cen J, Vornbrock AF, et al. High-speed printing of transistors: from inks to devices. *Proc IEEE*. 2015;103(4):567-582.

[28] Wang P, Chu W, Li W, et al. Three-dimensional laser printing of macro-scale glass objects at a micro-scale resolution. *Micromachines*. 2019;10(9):1-9.

[29] Pearre BW, Michas C, Tsang JM, Gardner TJ, Otchy TM. Fast micron-scale 3D printing with a resonant-scanning two-photon microscope. *Addit Manuf*. 2019;30:1-33.